

Deconvolution of continuous paleomagnetic data from pass-through magnetometer: A new algorithm to restore geomagnetic and environmental information based on realistic optimization

The Faculty of Oregon State University has made this article openly available.
Please share how this access benefits you. Your story matters.

Citation	Oda, H. & Xuan, C. (2014). Deconvolution of continuous paleomagnetic data from pass-through magnetometer: A new algorithm to restore geomagnetic and environmental information based on realistic optimization. <i>Geochemistry Geophysics Geosystems</i> , 15(10), 3907–3924. doi:10.1002/2014GC005513
DOI	10.1002/2014GC005513
Publisher	American Geophysical Union
Version	Version of Record
Terms of Use	http://cdss.library.oregonstate.edu/sa-termsfuse



RESEARCH ARTICLE

10.1002/2014GC005513

Special Section:

Magnetism From Atomic to Planetary Scales: Physical Principles and Interdisciplinary Applications in Geo- and Planetary Sciences

Key Points:

- Magnetometer sensor response is estimated reliably using a magnetic point source
- Magnetometer measurement noise is characterized by repeated data of a u-channel
- We show new deconvolution algorithm considering realistic measurement conditions

Supporting Information:

- Figures S1–S4
- Supplementary Figure Captions

Correspondence to:

H. Oda,
hirokuni-oda@aist.go.jp

Citation:

Oda, H., and C. Xuan (2014), Deconvolution of continuous paleomagnetic data from pass-through magnetometer: A new algorithm to restore geomagnetic and environmental information based on realistic optimization, *Geochem. Geophys. Geosyst.*, 15, 3907–3924, doi:10.1002/2014GC005513.

Received 21 JUL 2014

Accepted 25 SEP 2014

Accepted article online 4 OCT 2014

Published online 21 OCT 2014

Deconvolution of continuous paleomagnetic data from pass-through magnetometer: A new algorithm to restore geomagnetic and environmental information based on realistic optimization

Hirokuni Oda¹ and Chuang Xuan^{2,3}

¹Institute of Geology and Geoinformation, Geological Survey of Japan, AIST, Tsukuba, Japan, ²Ocean and Earth Science, National Oceanography Centre Southampton, University of Southampton, Southampton, UK, ³College of Earth, Ocean, and Atmospheric Sciences, Oregon State University, Corvallis, Oregon, USA

Abstract The development of pass-through superconducting rock magnetometers (SRM) has greatly promoted collection of paleomagnetic data from continuous long-core samples. The output of pass-through measurement is smoothed and distorted due to convolution of magnetization with the magnetometer sensor response. Although several studies could restore high-resolution paleomagnetic signal through deconvolution of pass-through measurement, difficulties in accurately measuring the magnetometer sensor response have hindered the application of deconvolution. We acquired reliable sensor response of an SRM at the Oregon State University based on repeated measurements of a precisely fabricated magnetic point source. In addition, we present an improved deconvolution algorithm based on Akaike's Bayesian Information Criterion (ABIC) minimization, incorporating new parameters to account for errors in sample measurement position and length. The new algorithm was tested using synthetic data constructed by convolving "true" paleomagnetic signal containing an "excursion" with the sensor response. Realistic noise was added to the synthetic measurement using Monte Carlo method based on measurement noise distribution acquired from 200 repeated measurements of a u-channel sample. Deconvolution of 1000 synthetic measurements with realistic noise closely resembles the "true" magnetization, and successfully restored fine-scale magnetization variations including the "excursion." Our analyses show that inaccuracy in sample measurement position and length significantly affects deconvolution estimation, and can be resolved using the new deconvolution algorithm. Optimized deconvolution of 20 repeated measurements of a u-channel sample yielded highly consistent deconvolution results and estimates of error in sample measurement position and length, demonstrating the reliability of the new deconvolution algorithm for real pass-through measurements.

1. Introduction

Superconducting rock magnetometers (SRM) are the most commonly used magnetometers in modern paleomagnetism studies [Goree, 2007]. SRM uses superconducting quantum interference devices (SQUIDS), superconducting magnetic flux transformers, and superconducting magnetic shielding operating at a liquid helium temperature of 4.2 K to measure the remanent magnetization in rock samples for paleomagnetic study. The first SRM was designed and installed at the University of Pittsburgh in 1970, which was horizontally orientated with a straight through, room temperature access [Goree and Fuller, 1976]. The use of SRMs for paleomagnetic measurement of continuous long core samples was first introduced by Dodson *et al.* [1974]. In 1985, the first long core SRM with radio frequency (RF) SQUIDS for continuous measurements was installed onboard the *R/V JOIDES Resolution* for the Ocean Drilling Program (ODP) and was later upgraded to direct current (DC) SQUIDS in 1992 for improved sensitivity [Goree, 2007]. The long core SRM systems have been routinely used by ODP and later by Integrated Ocean Drilling Program (IODP) expeditions to facilitate the timely construction of shipboard magnetostratigraphy.

In order to increase the spatial resolution of the traditional discrete paleomagnetic samples, Tauxe *et al.* [1983] introduced the continuous "u-channel" sample (typically $\sim 2 \times 2 \text{ cm}^2$ cross section, 150 cm long). U-channels are usually taken from the pristine central part of half-core sections, away from the often-

disturbed outer part of cores that may considerably degrade the paleomagnetic measurement [Acton *et al.*, 2002]. The first “U-channel” SRM with higher-resolution pickup coils (due to the smaller diameter of u-channels relative to half-core sections) was introduced in 1991 [Weeks *et al.*, 1993]. Since then, over twenty u-channel SRM systems have been installed at worldwide paleomagnetism research laboratories. Developments in long core and u-channel SRM systems during the last few decades have led to fast accumulation of paleomagnetic data from continuous sediment samples that have greatly contributed to high-resolution full vector reconstruction of Earth’s past magnetic field [e.g., Weeks *et al.*, 1993; Channell *et al.*, 1997; Roberts, 2006; Ohno *et al.*, 2008]. For instance, stacked records of paleointensity reconstructions, obtained mostly from continuous core sample measurements, have provided valuable information about the dipole field evolution while serving as high-resolution environmentally independent stratigraphy tool for correlating and dating worldwide sediment sequences [e.g., Guyodo and Valet, 1999; Valet *et al.*, 2005; Channell *et al.*, 2009].

As paleomagnetic data acquired from continuous samples on pass-through SRM are smoothed and distorted due to convolution effect of the magnetometer sensor response, deconvolution is necessary to restore the magnetization at resolution comparable to that measured using side-by-side discrete samples. Although sediment magnetization lock-in process may lead to time delay and smoothing of sedimentary paleomagnetic records [e.g., Channell and Guyodo, 2004; Saganuma *et al.*, 2011], further smoothing introduced during pass-through measurements usually distort paleomagnetic signals significantly for samples deposited at a wide range of accumulation rates. Therefore, reliable deconvolution is often desirable to improve the data resolution. Dodson *et al.* [1974] conducted deconvolution of pass-through paleomagnetic data utilizing Fast Fourier Transform (FFT) with low-pass filter on axial component of measured magnetization, with optimum filtering empirically determined by the user. Constable and Parker [1991] introduced a deconvolution algorithm based on a smoothness-constrained least-squares method by estimating system noise level using measurements made beyond the continuous sample (i.e., leader and trailer). Oda and Shibuya [1994] conducted optimized deconvolution incorporating a smoothness-constrained least-squares method based on Akaike’s Bayesian Information Criterion (ABIC) minimization, which was later extended to 3-D with cross terms by Oda and Shibuya [1996]. The cross terms have been proved to be particularly important to deconvolve measurements made on the SRM onboard *R/V JOIDES Resolution*, where half-round core samples occupy only the lower half of the pickup coils during the measurements [e.g., Oda *et al.*, 2000]. Guyodo *et al.* [2002] successfully applied the deconvolution scheme of Oda and Shibuya [1996] and restored a short excursion event from a u-channel measurement that was not recognized before the deconvolution.

Jackson *et al.* [2010] summarized five basic assumptions of pass-through measurements for deconvolution with better accuracy and reliability: (a) measurement errors follow Gaussian distribution with zero mean and are independent of measurement position; (b) magnetization in sample varies only as a function of depth; (c) variations in magnetizations are smooth and the smoothness of the magnetization is similar throughout the core; (d) the length and sample position of the measurement are accurately known; and (e) the magnetometer sensor response function is accurately known. In this paper, we present an improved deconvolution algorithm considering assumptions (a), (d) and (e). First, we acquired an accurate estimate of magnetometer sensor response through repeated measurements of a carefully designed magnetic point source sample. Second, based on 200 repeated measurements for an ~1.49 m long u-channel sample, characteristics of SRM measurement noise were analyzed and used to produce realistic measurement noise for testing reliability of deconvolution algorithms. Third, we recognize that it is common to have errors (a few mm to few cm) in sample length and position during a continuous pass-through measurement, and developed an ABIC minimization based deconvolution algorithm [e.g., Oda and Shibuya, 1994, 1996, 1998] that overcomes such errors. Finally, we demonstrate the validity and robustness of the new deconvolution algorithm using synthetic data containing a geomagnetic excursion with realistic measurement noise, and repeated measurements of an actual u-channel sample.

2. Response Function Determination

2.1. General Idea and Previous Methods

SRMs normally use three orthogonal superconducting pickup-coil pairs arranged about a center measurement position. The axial pickup coils are designed according to the Helmholtz configuration [Helmholtz,

1849] to maximize the homogeneity for the space occupied by a discrete paleomagnetic sample, and the transverse pickup coils are typically saddle-shaped coils. *Oda and Shibuya* [1996] expressed the pass-through measurements of a continuous sample on an SRM as below,

$$\mathbf{d} = \mathbf{R}\mathbf{m} + \varepsilon \quad (1)$$

where \mathbf{d} is the pass-through measurements, \mathbf{R} is the empirically measured sensor response, \mathbf{m} is the magnetization of the continuous sample, and ε is the noise, respectively. ε equals $-\delta\mathbf{R}\mathbf{m} + \mathbf{e}$, where $\delta\mathbf{R}\mathbf{m}$ is the error originating from the uncertainty of sensor response and \mathbf{e} is the true measurement noise. Apparently, systematic error in determining the sensor response may lead to undesired effects on deconvolution. The sensor response of a particular SRM will likely remain unchanged for relatively long time. It is therefore beneficial to accurately estimate the sensor response function of an SRM, which can be repeatedly used for deconvolution of pass-through measurements made on that SRM.

The sensor response function of an SRM is primarily determined by the geometry of the sensing coils, while “image effects” produced by the superconducting shield (used to maximize the sensitivity and minimize the noise of the SQUID system) may complicate the actual response [e.g., *Zięba*, 1993]. *Shibuya and Michikawa* [2000] performed theoretical calculations of sensor response for the first generation SRM onboard *R/V JOIDES Resolution* with superconducting shield, and obtained results comparable to the empirical measurement along z axis [*Oda and Shibuya*, 1996]. However, the derived sensor response significantly deviated from the measured response in x and y axes, possibly due to imperfect geometry and potential offset of the pickup coils from the geometrical center. Similarly, *Parker and Gee* [2002] measured the sensor response of the second generation SRM onboard *R/V JOIDES Resolution* and noticed that the centers of x and z axis pickup coils are displaced from the geometric center by ~ 0.7 cm. The discrepancy of the theoretical sensor response from the actual response leads to distortion of the deconvolved magnetization, which could only be recognized with accurate estimates of the sensor response. Various methods and materials have been used for empirical determination of SRM sensor response. For instance, estimate of the sensor response of the first generation SRM onboard *R/V JOIDES Resolution* by *Oda and Shibuya* [1996] used magnetic tape with the cross sectional shape of a half-round sample. *Jackson et al.* [2010] estimated sensor response function based on six scans of a homogeneous specimen ($18 \times 18 \times 15$ mm³) and used equation (1) to calculate \mathbf{R} from measurement \mathbf{d} and magnetization \mathbf{m} . *Parker and Gee* [2002] measured the sensor response using a small dipole standard sample placed in a cylindrical plexiglass holder, which was fitted into one of the holes in the holder (z axis), or taped (x and y axes) to the surface of the holder. To increase the accuracy of orientation, and to avoid heterogeneity of the specimen, we use a dipole magnetic point source fixed in the center of a polycarbonate cube for sensor response measurement.

2.2. Response Function Determination With a Magnetic Point Source

In this paper, we used the u-channel SRM (2G model 755–1.65UC) at Oregon State University (OSU) for measurements of sensor response function and magnetizations of u-channel samples (Figure 1a). The pickup coil design of the u-channel SRM at OSU is essentially the same as that of the first u-channel SRM introduced by *Weeks et al.* [1993], as well as that of the u-channel SRM used by *Jackson et al.* [2010]. The axial (z) coils of the OSU magnetometer are circular, with a diameter of ~ 85 mm, and the transverse sensors are saddle coil pairs, formed on the same cylindrical core. The axial-coil pair separation (D) is ~ 24 mm, and the saddle coils have a length (L) of ~ 68 mm. This geometry is intermediate between the “high homogeneity” arrangement ($D = 40$ mm, $L = \sim 100$ mm) optimized for discrete sample measurements and the “high-resolution” geometry ($D = 20$ mm, $L = \sim 40$ mm) designed for maximum resolution [*Jackson et al.*, 2010]. The coordinate system of the magnetometer at OSU is shown in Figure 1a.

In order to acquire a reliable estimate of magnetometer sensor response, we prepared a polycarbonate cube with 5 mm edge length that includes a magnetic point source in the center of the cube. The point source carries a stable remanent magnetization perpendicular to one surface of the cube (Figure 1b). Deviations of the cube surfaces from perfect orthogonality are $\sim 0.5^\circ$, allowing the point source magnetization to be accurately aligned in the three orthogonal directions. We made the magnetic point source using a powder of plastic magnet ($H_c = 890$ mT, $H_{cr} = 894$ mT) and instant glue. A pulsed magnetic field of 2.5 T was applied three times while the instant glue was hardening. The point source was subsequently demagnetized using alternating field (AF) with a peak field of 50 mT, and magnetic moment of the point source (declination = 1.5° , inclination = 1.0° , magnetic moment = $6.17 \pm 0.15 \times 10^{-6}$ Am²) was measured on a

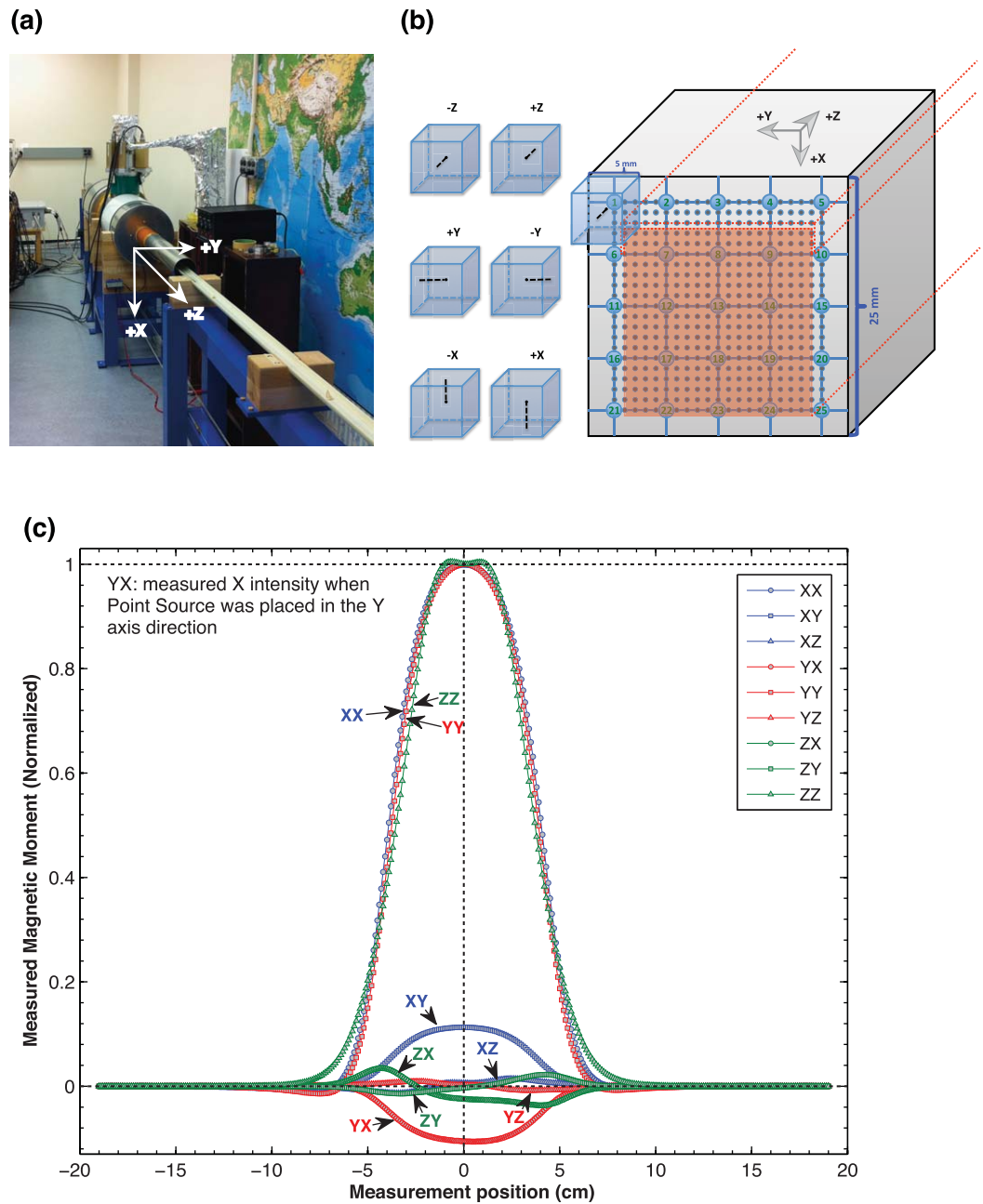


Figure 1. (a) SRM at Oregon State University (OSU) with coordinates indicated by white arrows. (b) Illustration of magnetic point source measurement procedure with coordinates indicated by arrows. Oriented magnetic point source is fixed in the center of a polycarbonate cube (5 mm edge length) that was attached to a larger polycarbonate cube (25 mm edge length) during the measurement. One surface of the larger cube marks 25 evenly spaced grid positions. Gray circles are interpolated 1 mm grid points, and shaded area indicates the cross section of a u-channel (18×18 mm²) used for integration. (c) Sensor response after u-channel cross-area integration for each 1 mm measured positions along Z axis. "AB" in legend means sensor response of "B"-axis pickup coil to magnetization oriented along "A" axis, where "A" and "B" are either "X," "Y," or "Z."

spinner magnetometer at the Geological Survey of Japan (model SMM-85, Natsuhara Giken; cross calibrated using a standard coil and current with an error < 1%). The point source was mounted using thin double-sided tape onto one surface of a larger polycarbonate cube (25 mm edge length) with 5 × 5 grids marked at every 5 mm intervals. The large polycarbonate cube was tightly attached to the measurement tray using double-sided tape. Another rectangular rod was used to align the point source cube precisely parallel to the grids. The angular errors of the small cube with point source relative to the large cube is expected to be around 1°. The point source was repeatedly measured (a total of 150 times) over an ~40 cm interval along

the track at every 1 mm intervals, while placed at each of the 25 grid positions orienting parallel or antiparallel to each of the three orthogonal axes (Figure 1b).

The peak reading of magnetic moment of the point source at position "13" (Figure 1b) in z axis pick up coil is $6.12 \times 10^{-6} \text{ Am}^2$, which is highly consistent with that measured on the spinner magnetometer, agreeing with the fact that 2G magnetometers are calibrated with a standard coil and current before delivery [William Goree; *personal communication*]. The peak reading of magnetic moment observed at position "13" in z axis pick up coil was used to normalize the sensor response curves measured at each grid position (Supporting information Figure 1). To estimate sensor response over the cross area of a u-channel sample ($\sim 18 \times 18 \text{ mm}^2$), we first interpolated the 5×5 grid response measurements with 5 mm spacing to 1 mm spacing (i.e., 21×21 grids) using spline functions, and then calculated the integrated sensor response over the u-channel cross area (red shaded area in Figure 1b). The integrated sensor response was further normalized by the cross area and presented in Figure 1c. The x-y and y-x cross terms contribute significantly to the sensor response. Deconvolution with and without y cross terms on a u-channel with comparable magnetizations along three axes show significant differences (Supporting information Figure 2), and suggest an $\sim 6^\circ$ rotation of x-y pickup coils around the z axis relative to the plane of the measurement tray. Similar rotation (about 2.4°) around the z axis was previously reported by Parker and Gee [2002] for the SRM onboard R/V JOIDES Resolution. Jackson et al. [2010] also observed nonnegligible components in x-y and y-x cross terms for SRM at the Institute for Rock Magnetism (IRM).

3. Improvements in Deconvolution Algorithm

The deconvolution algorithm in this paper is based on equations described by Oda and Shibuya [1996]. Major modifications and improvements in this study include: (1) consideration of cross terms related to y axis, (2) measurements are considered to start from the edge of a sample, (3) incorporation of position shift of a sample relative to the actual measurement start line, and (4) correction for error in sample length used for measurement. Figure 2 explains the difference between the algorithm of Oda and Shibuya [1996] and this study in measurement points (solid circles) and the representative center points (open circles) of uniformly magnetized slices. Oda and Shibuya [1996] assumed that measurement points start from the position half the measurement interval inside from the measurement "Start Line" on the tray for a u-channel. In this study, pass-through measurement is assumed to start from the measurement "Start Line", which is usually the case for measurements collected using 2G software. As a result, a 150 cm long u-channel measured at every 1 cm interval will have a total of 151 measurement points, with the first and last measurement points centered at the two ends of the u-channel. Note that the first and last slices (both enclosed by broken lines in Figure 2) are half filled with sediments.

Due to potential errors in placing the sample and in measurement start line calibration, or small void space at the beginning of sample, a relative shift may exist between the "Start of Sediment" and the actual measurement "Start Line" during pass-through measurement (Figure 2c). In our algorithm, a potential gap between "Start of Sediment" and actual measurement "Start Line" ("Gap" in Figure 2c) including void space in the first slice are accommodated using a new parameter "position shift" (δ) of the sensor response (Figure 2d). Furthermore, sample length used for pass-through measurement may not exactly reflect the actual sample length. For instance, a u-channel sample with actual sediment length of 149.6 cm could be measured as 150 cm long yielding a total of 151 measurement points. This difference between actual sample length and measurement length as well as a "Gap" between "Start of Sediment" from "Start Line" results in varying proportion of sediment filling the last slice (0–1). Thus, we introduce additional new parameters w_s and w_e to represent "length correction" for the first and last slices needed to adjust the measurement length to actual sample length.

Oda and Shibuya [1996] omitted cross terms of sensor response related to the y axis (i.e.; x-y, y-x, y-z, z-y terms) for deconvolution, with the assumption that samples move right along the centerline of pickup coils and the coils were perfectly wound. Precise sensor response measurements from this study (Figure 1c) and previous studies [Parker and Gee, 2002; Jackson et al., 2010] revealed that the cross terms are not negligible. Therefore, in this study we use the full tensor of sensor response for deconvolution. The basic formulae on pass-through measurement on a pass-through SRM (equation (1)) can be expressed in three axes as below,

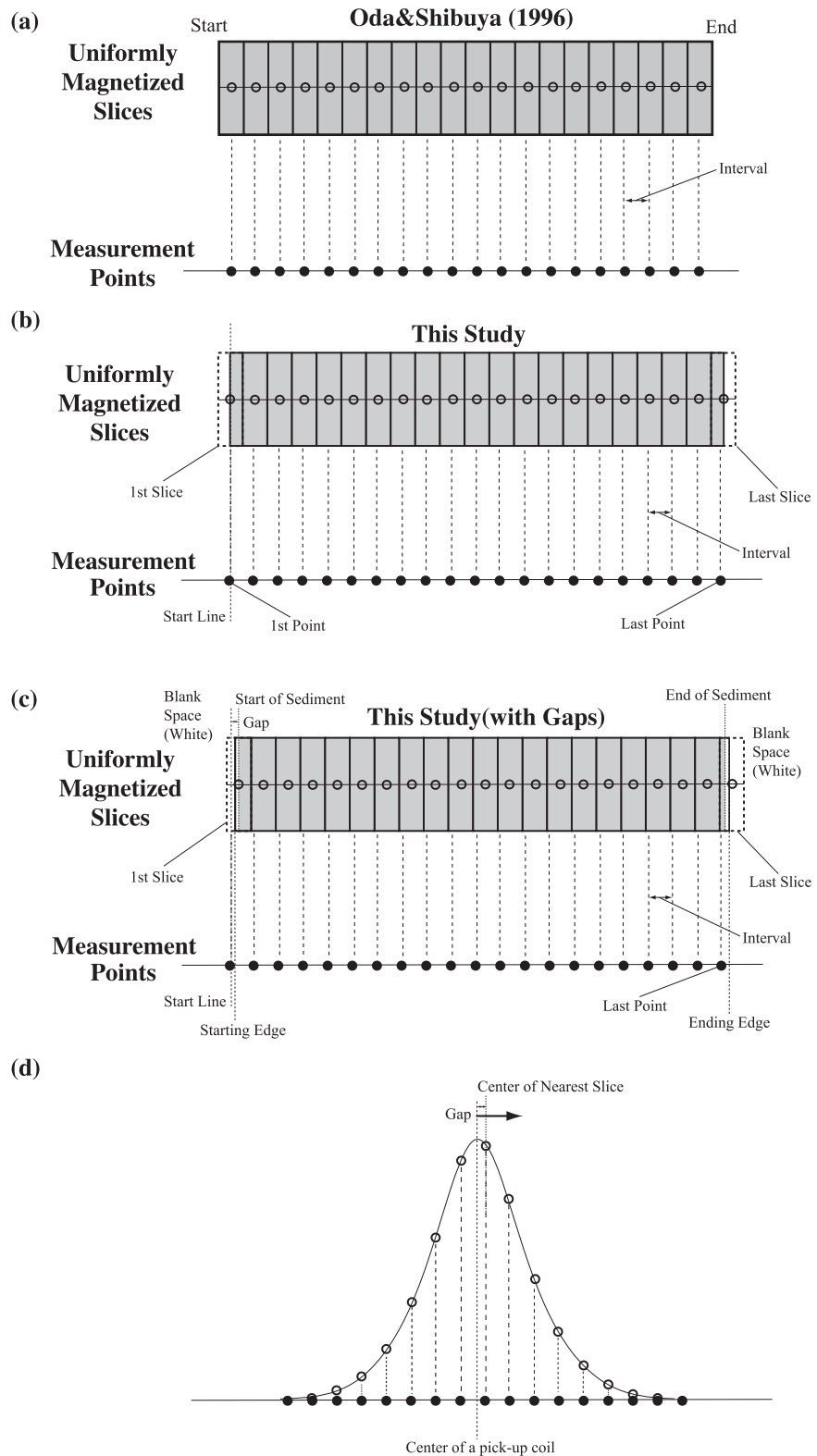


Figure 2. Illustrations on the measurement points (solid circles) and the center (open circles) of uniformly magnetized slices used for the algorithm of (a) *Oda and Shibuya* [1996] and (b) this study. (c) Illustration of measurements with gaps/spaces in the first and last slices. (d) Illustration of sensor response functions used for the deconvolution in this study. Gray shaded parts represent the space filled with sediments, and each rectangle represents uniformly magnetized slice of a u-channel.

$$\begin{bmatrix} \mathbf{d}_x \\ \mathbf{d}_y \\ \mathbf{d}_z \end{bmatrix} = v \begin{bmatrix} R_{xx} & R_{yx} & R_{zx} \\ R_{xy} & R_{yy} & R_{zy} \\ R_{xz} & R_{yz} & R_{zz} \end{bmatrix} \mathbf{f} \begin{bmatrix} \mathbf{m}_x \\ \mathbf{m}_y \\ \mathbf{m}_z \end{bmatrix} + \begin{bmatrix} \varepsilon_x \\ \varepsilon_y \\ \varepsilon_z \end{bmatrix} \quad (2)$$

where subscripts in \mathbf{d}_b , \mathbf{m}_a and ε_b correspond to the vector component in axis a or b ($a=x, y, \text{ or } z; b=x, y, \text{ or } z$) [see Oda and Shibuya, 1996]. Lengths of \mathbf{d}_b and ε_b equal the number of measured points (N), and length of \mathbf{m}_a equals the number of unit slices (M). R_{ab} is the sensor response term produced by the a axis component of magnetization in the b axis pickup coil integrated over a unit slice and normalized by the volume of the slice. Matrix R_{ab} has M columns and $(M + ll + lt)$ rows, where ll and lt are the numbers of leader and trailer measurements, respectively. Different to that in Oda and Shibuya [1996] where leader and trailer length are fixed to be the same, the new algorithm allows different measurement points for leader and trailer to increase the freedom. The position of sensor response data is flipped for deconvolution, because the sensor response measured first is the last of the sensor response for the convolution of magnetization.

\mathbf{f} in equation (2) is the matrix representing sediment fill ratio of each unit sample slice. v is the volume of a unit slice expressed as $v = s \cdot h$, where s is the cross sectional area of a u-channel, and h is the measurement interval, which is constant and equal to the thickness of a unit slice. The matrix of sediment fill ratios \mathbf{f} in equation (2) can be expressed as follows,

$$\mathbf{f} = \begin{pmatrix} \mathbf{f}_1 & \mathbf{0} & \mathbf{0} \\ \mathbf{0} & \mathbf{f}_1 & \mathbf{0} \\ \mathbf{0} & \mathbf{0} & \mathbf{f}_1 \end{pmatrix}, \quad \mathbf{f}_1 = \begin{pmatrix} 0.5+w_s & & & \\ & 1 & & \mathbf{0} \\ & & \ddots & \\ & \mathbf{0} & & 1 \\ & & & & 0.5+w_e \end{pmatrix} \quad (3)$$

Contributions of the magnetization \mathbf{m} from the starting and ending slices to the measurements are reduced according to the length corrections w_s and w_e . According to the proportion of sediment filling the first and last slices, w_s and w_e are assumed to change between -0.5 (empty) and $+0.5$ (full). If the first or last slice is half filled with the sediment as a default condition, w_s and w_e both equal zero.

Measurement noises in the three orthogonal axes are assumed to be Gaussian distributed with mean of zero and variance of v , and are independent from each other (i.e., noise originated from sensor response and/or positioning error is negligible). The likelihood function of a pass-through measurement is

$$L(\mathbf{d}|\mathbf{m}, v) = \left(\frac{1}{2\pi v}\right)^{\frac{3N}{2}} \exp\left\{-\frac{1}{2v} \|\mathbf{d} - v\mathbf{Rf}\mathbf{m}\|^2\right\} \quad (4)$$

where $\|\mathbf{a}\|^2$ represents Euclidean norm of vector \mathbf{a} . A simple maximum likelihood solution can be obtained by minimizing $\|\mathbf{d} - v\mathbf{Rf}\mathbf{m}\|^2$.

Following Oda and Shibuya [1996], the solution of equation (4) is stabilized by assuming that the magnetization change smoothly which was measured by the L_2 norm of second-order difference. The matrix formulation of the second-order difference is $\|\mathbf{z} - \mathbf{Dm}\|^2$, where \mathbf{D} and \mathbf{z} are the same as in Oda and Shibuya [1996]. The second-order differences are assumed to be Gaussian distributed with zero mean and a variance of v/u^2 , where u is the hyper-parameter that measures the smoothness of the magnetization. With increasing u , the magnetization is forced to change more smoothly. Using the matrix expression above, the prior distribution of magnetization \mathbf{m} is given by

$$p(\mathbf{m}|v, u) = \alpha \left(\frac{u^2}{2\pi v}\right)^{\frac{3M}{2}} |\mathbf{D}^t \mathbf{D}|^{\frac{1}{2}} \exp\left\{-\frac{u^2}{2v} \|\mathbf{z} - \mathbf{Dm}\|^2\right\} \quad (5)$$

Following the formulae provided by Oda and Shibuya [1996], ABIC is calculated as below

$$ABIC = 3M \log\left(\frac{2\pi S^*}{3N}\right) + 3N - 3M \log(u^2) - \log|\mathbf{D}^t \mathbf{D}| + \log|\mathbf{F}^t \mathbf{F}| + 2K \quad (6)$$

where $S^* = \|\mathbf{b} - \mathbf{Fm}_0\|^2$, $\mathbf{b} = \begin{bmatrix} \mathbf{d} \\ u\mathbf{z} \end{bmatrix}$, $\mathbf{F} = \begin{bmatrix} v\mathbf{Rf} \\ u\mathbf{D} \end{bmatrix}$, \mathbf{m}_0 is \mathbf{m} that minimizes $S = \|\mathbf{b} - \mathbf{Fm}\|^2$, and K is the number

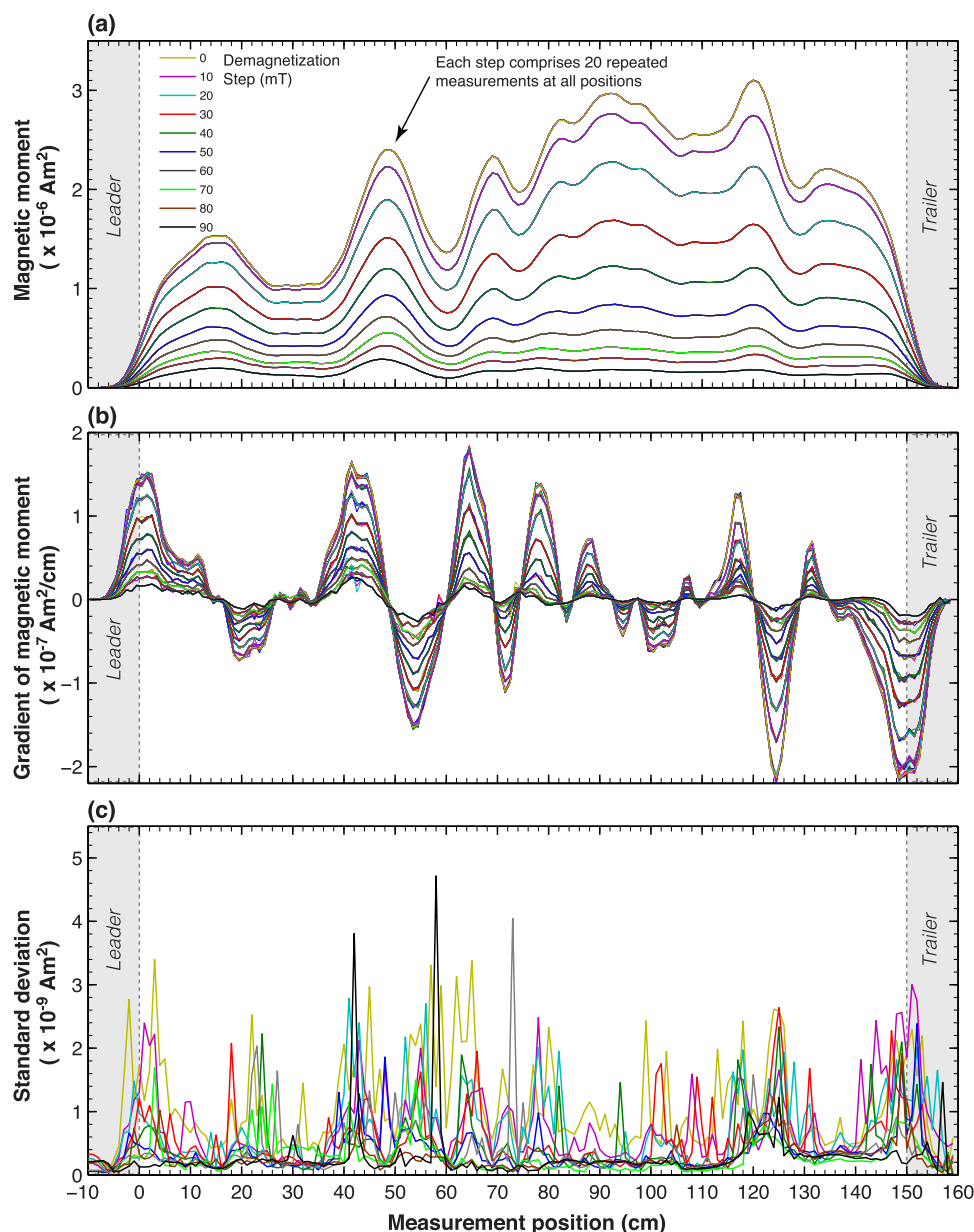


Figure 3. (a) Magnetic moments and (b) gradient of measured magnetic moments of 200 repeated measurements for u-channel sample “EW0408-95JC-6.” The sample was repeatedly measured 20 times after each of the ten AF demagnetization treatments from 0 to 90 mT at 10 mT steps. (c) Standard deviation of magnetic moments for 20 repeated runs calculated for each demagnetization step in (a).

of parameters and is set as 4 in our case that corresponds to u , δ , w_s , and w_e , although w_s is fixed to 0. Minimization of S^* and error calculations were conducted as matrix calculations similar to that of Oda and Shibuya [1996]. After the matrix calculation, ABIC is calculated and the optimum solution was obtained by minimizing ABIC against three parameters; u , δ and w_e . In practice, the position shift (δ) and length correction of the last slice (w_e) should be the same for the same sample measured at different demagnetization steps, if the sample was not moved between measurement steps.

4. Investigations on Uncertainties in SRM Measurement

Uncertainty in continuous measurements on the SRM at OSU was investigated utilizing a total of 200 repeated NRM measurements of an ~1.49 m long u-channel sample collected from core section EW0408-95JC-6 (Latitude: 60.663°, Longitude: -147.709°, Water Depth: 744 m) that comprises mainly silty clay

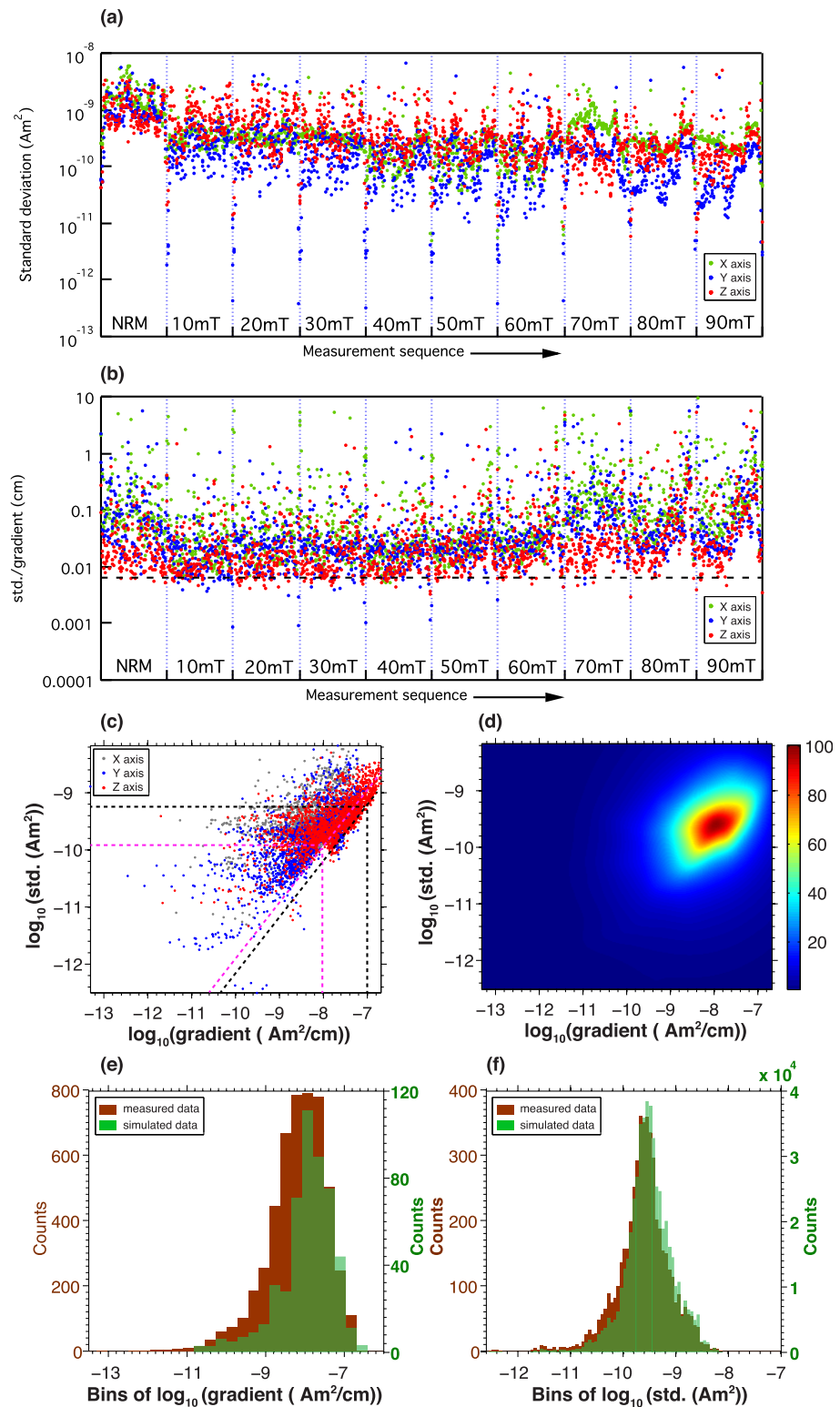


Figure 4. Standard deviation (std.) and absolute gradient of measured magnetic moment from repeated measurements of u-channel sample “EW0408-95JC-6” and simulated data used in Figure 5. (a) Std., and (b) std./gradient versus measurement sequence for the three measurement axes on logarithmic scale. Data for x, y, and z axes are in green, blue, and red, respectively. Each rectangular block between two vertical dashed lines contains data from one demagnetization step. Horizontal dashed line represents value corresponding to std./gradient value of 0.006 cm. (c) Log-log plot of std. versus gradient of measured magnetic moment. Gray, blue, and red dots correspond data from x, y, and z axes, respectively. (d) Color contour showing density of data in (c), where red (blue) shows maximum (minimum) data density. Histograms of (e) gradient and (f) std. of magnetic moment for measured data (red) and simulated data (green) for all three axes and demagnetization steps combined. Horizontal axes of the histograms are on logarithm scale.

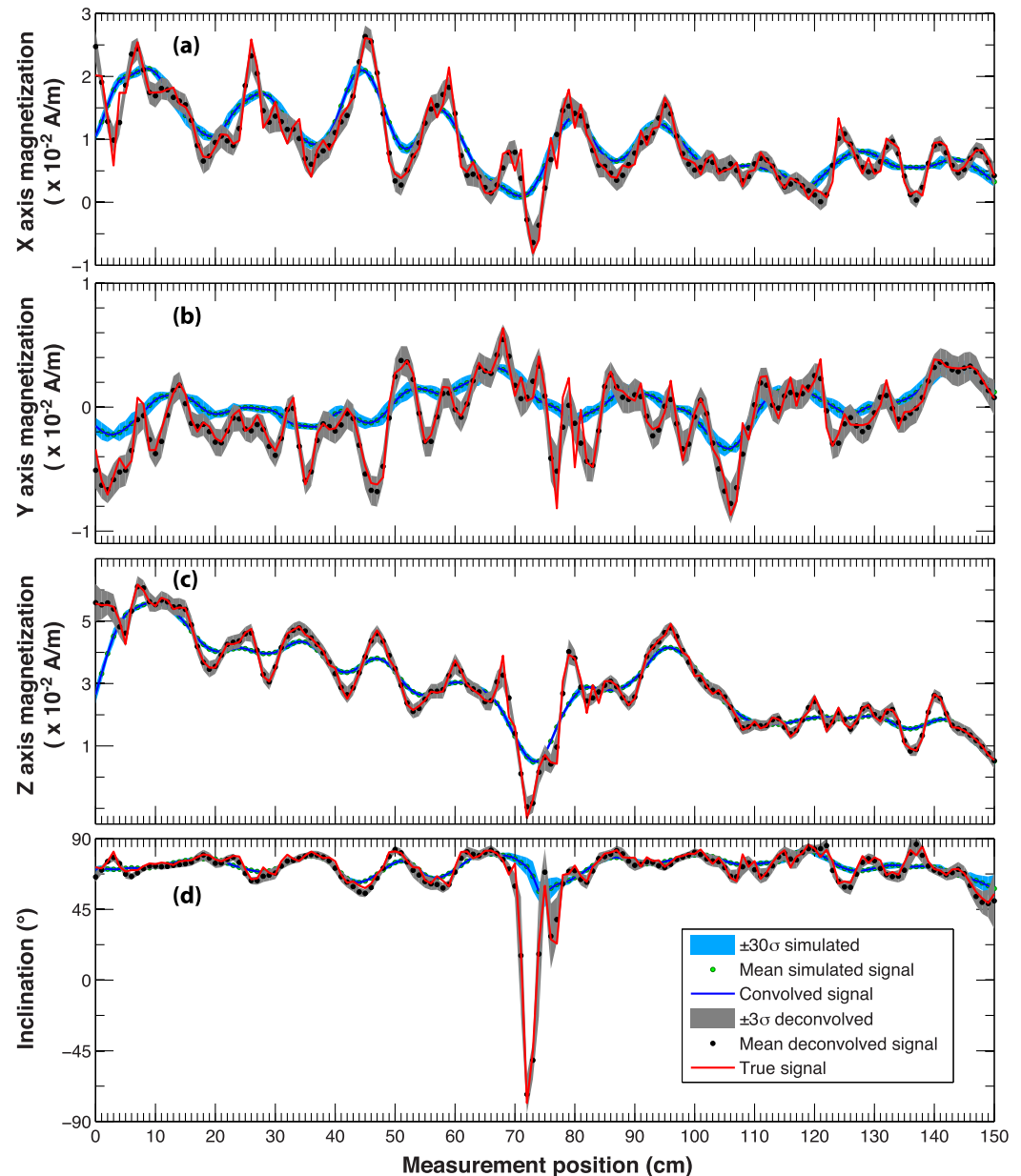


Figure 5. Synthetic measurement data with simulated noise before and after deconvolution compared with “true” signal (red curve) in (a) x, (b) y, and (c) z axis, and (d) inclination. Mean and 3σ of 1000 simulated magnetization was shown as green circles and blue shaded area, respectively. Mean and 3σ of the 1000 deconvolved signal were shown as black circles and gray shaded area, respectively. Conversion from magnetic moment to magnetization was done by normalizing the magnetic moment by the cross section area of a u-channel and the effective lengths of sensor responses along track.

sediments. Measurements were made at every 1 cm interval for the u-channel as well as 10 cm before (“leader”) and 10 cm after (“trailer”) the u-channel. NRM measurements after AF demagnetization with peak fields from 0 to 90 mT at 10 mT steps were used here for analyses. Measurements for each demagnetization step comprise 20 consecutive repeated runs. A modified version of the UPmag software [Xuan and Channell, 2009] was used to correct flux jumps and spike noises in the measurements. The total magnetic moments of the 200 repeated measurements are shown in Figure 3a. The consecutive 20 repeated runs for each demagnetization step are highly consistent with each other with deviations typically less than 0.1% of the mean magnetic moment, and are often invisible due to the thickness of the colored lines in Figure 3a.

Figure 3b shows the gradient of measured magnetic moment for each run. Absolute gradient of measured magnetic moment seems to increase at both ends of the u-channel. Measurement

positions with minimum gradient of measured magnetic moment are consistent through demagnetization steps up to 90 mT. Standard deviation of 20 measurements for each demagnetization step is shown in Figure 3c. In general, standard deviations are at least three orders of magnitudes lower than the magnetic moment indicating excellent repeatability of measurements for each demagnetization step. It appears that significant peaks in standard deviation correspond to positions with larger absolute gradient of measured magnetic moment. Possible relation between measurement error and gradient of measured magnetic moment was pointed out by Jackson *et al.* [2010] (e.g., Figures 4 and 5). Our data confirm such a relation with observations on 20 repeated measurements for each of the 10 demagnetization steps.

Figures 4a and 4b show std. and std./gradient variations of all 200 runs for each individual axis. In general, standard deviations decrease with stepwise AF demagnetization. Standard deviations of measurements before demagnetization (NRM) appear significantly larger than those after demagnetization (10 mT and further), which could be related to decay of viscous remanence through 20 repeated measurements of NRM starting from the initial insert of u-channel to the SRM. Std./gradient data show higher value before demagnetization, and seem to increase with increasing demagnetization levels from ~60 mT to 90 mT. The wedge shaped area void of data for 80 mT and 90 mT steps could indicate increase in drift noise relative to the magnetic moment with 1/f character that is typical for SRM [Jackson *et al.*, 2010]. Distribution of data points on the diagram of std./gradient show a lower limit at around 0.06 mm (horizontal broken line in Figure 4b) that could be close to the standard deviation of position error in the normal SRM measurement state. There might be larger episodic position errors of 'stop and go' mode related to the friction between the tray and the track, which is sometimes witnessed during measurements.

Figure 4c shows a log-log plot of standard deviation against gradient of measured magnetic moment. A wedge-shaped area with no data presents below the scattered data points, suggesting that the minimum of standard deviation increases with gradient of measured magnetic moment. This clearly indicates that measurement error is significantly related to the gradient of measured magnetic moment, likely due to positioning error. The thick dashed black line in Figure 4c marks the bottom line of the distribution of the standard deviation. The line has a slope of unity (linear relationship) and goes through a point of $\log_{10}(\text{std.}) = -9.2$ and $\log_{10}(\text{gradient}) = -7$, which again corresponds to a minimum estimate of positioning error of 0.06 mm. The dashed magenta line in Figure 4c shows the bottom line of the distribution of the standard deviation corresponding to the lower value of the gradient of measured magnetic moment. The line has a slope of unity and goes through a point of $\log_{10}(\text{std.}) = -9.9$ and $\log_{10}(\text{gradient}) = -8$, corresponding to a minimum positioning error of 0.12 mm.

According to Jackson *et al.* [2010], measurement error $\bar{\sigma}_D$ can be formulated as below,

$$\bar{\sigma}_D(z) = \bar{\sigma}_0 + \sigma_z d\bar{D} / dz \tag{7}$$

where $\bar{\sigma}_0$ is the noise of SRM excluding linear drift, σ_z is the positional error, and $d\bar{D} / dz$ is the gradient of measured magnetic moment along the track. Jackson *et al.* [2010] estimated positioning error from the slope of std. versus gradient, and system noise from the intercept based on equation (7). Density distribution of all three axes (Figure 4d) data has peaks of standard deviation around $2.5 \times 10^{-10} \text{ Am}^2$ and gradient around $1 \times 10^{-8} \text{ Am}^2/\text{cm}$, which can also be recognized as modes on histograms of gradient (Figure 4e) and standard deviation (Figure 4f). The histograms in each axis exhibit different distribution, and z axis has modes on standard deviation of $\sim 1.2 \times 10^{-10} \text{ Am}^2$ and std./gradient of $\sim 9 \times 10^{-3} \text{ cm}$. A preliminary forward modeling on the distribution of standard deviation versus gradient in z axis based on equation (7) shows that modes on the histograms of standard deviation and std./gradient could be reasonably reconstructed with $\sigma_0 = 1.2 \times 10^{-10} \text{ Am}^2$ and $\sigma_z = 9 \times 10^{-3} \text{ cm}$. However, the model could not accommodate standard deviation higher than the mode very well. This might be caused by non-Gaussian distributed noise components (e.g., instrument noise and/or position error). For instance, Jackson *et al.* [2010] pointed out that measurements on SRM exhibit drift with 1/f frequency distribution longer than 30 s. In addition, position error may increase due to the extension of the handler rope away from the home position, and noise in one axis may originate from other axes through cross terms of sensor response.

5. Test Using Synthetic Data

5.1. Reliability of Deconvolution With Realistic Noise

In order to demonstrate the robustness of the improved deconvolution scheme, we conducted deconvolution on synthetic signal with simulated noise. We constructed a “true” vector signal (red curves in Figure 5) based on a high-resolution record of Iceland Basin excursion recorded at ODP Site 983 [Channell *et al.*, 1997]. The “true” signal was then convolved with the well-estimated OSU magnetometer sensor response function (Figure 1c), to produce a synthetic “measured” signal (blue curves in Figure 5). The mean of the total magnetic moments of the synthetic “measured” signal was adjusted to be the same as the mean of the 200 repeated measurements of EW0408-95JC-6. The distribution of the gradients of magnetic moment of the synthetic signal is similar to that of the measured data from EW0408-95JC-6 (Figure 4e). The synthetic signal therefore provides a realistic representation of actual measurement data.

Realistic noise was produced by 1000 runs of Monte Carlo simulation and added to the synthetic magnetic moment signal. We assume measurement noise is related to the gradient of magnetic moment signal. For each synthetic measurement position, standard deviations of measurement error on each axis were randomly drawn based on the gradient of the synthetic signal on that axis, and the standard deviation versus gradient relation defined by the total number of 5070 (169 measurement points \times 10 demagnetization steps \times 3 axes) data points in Figure 4c. The distribution of the standard deviation of measurement errors from the 1000 simulations is shown in Figure 4f (in green). The simulated noise distribution clearly resembles that based on actual measurement (in red). The means of 1000 simulated magnetic moment signals are shown as green circles in Figure 5. The blue shaded area in Figure 5 represents a $\pm 3\sigma$ range from the mean magnetic moment.

Each of the 1000 simulated measurements was deconvolved separately with optimization on $\ln(u)$, and the mean and $\pm 3\sigma$ ranges of the 1000 deconvolved magnetizations are shown as black circles and gray shading in Figure 5, respectively. Note the similarities between the “true” signal (red curves) and the deconvolved signal (black circles with gray shading). The “true” magnetization is mostly within the $\pm 3\sigma$ range for the deconvolved signal. It is clear that the synthetic geomagnetic excursion constructed based on real data was not visible before deconvolution, and was successfully restored after deconvolution. Smaller amplitude fluctuations with spatial resolution higher than the sensor response (typically ~ 4 cm) were apparently smoothed out in the synthetic measurements, but were successfully recovered after deconvolution.

Comparison of the estimated residual and simulated residual (Supporting information Figure 2) shows that the mean of the 1000 simulated “true” residual is mostly close to zero on all three axes, whereas the mean of the 1000 estimated residual changes with measurement position. The larger deviation of the mean estimated residual from zero at certain measurement positions could be caused by the roughness of the simulated model magnetization. For most of the measurement positions, $\pm \sigma$ of the simulated residual is larger than that of the estimated residual, possibly because the optimized model magnetic moment is closer to the simulated magnetic moment with noise than to the true magnetic moment. Larger residuals around 0 cm in the z axis and around 70–80 cm in the x and z axes (corresponding to the simulated geomagnetic excursion interval) are associated with larger amplitudes in the gradient of measured magnetic moment (Supporting information Figure 2d) that potentially produce larger error according to Figure 4b.

We also compared the standard deviation of error estimated by the deconvolution algorithm (based on Oda and Shibuya [1996, equation (18)]) with the “true” standard deviation of error calculated from the difference between the deconvolved data and the “true” magnetization (Supporting information Figure 3). The estimated error standard deviation agrees well with the calculated error standard deviation on the y axis, with generally lower values in the estimated error standard deviation. The estimated error standard deviation deviates significantly from the calculated error standard deviation on the x axis, especially for the first half of the u-channel. For the z axis, the calculated error std. is much larger than estimated error std., and shows prominent peaks at ~ 0 cm and ~ 70 –80 cm. The large discrepancy on the x and z axes might be explained by the larger gradient of measured magnetic moment for the corresponding intervals on the two axes (Supporting information Figure 3d), which may introduce larger amplitude non-Gaussian noise based on Figure 4b. Although the assumption of a Gaussian distribution for the measurement noise in equation (4) was not satisfied completely, the deconvolved magnetizations for 1000 simulated measurements are

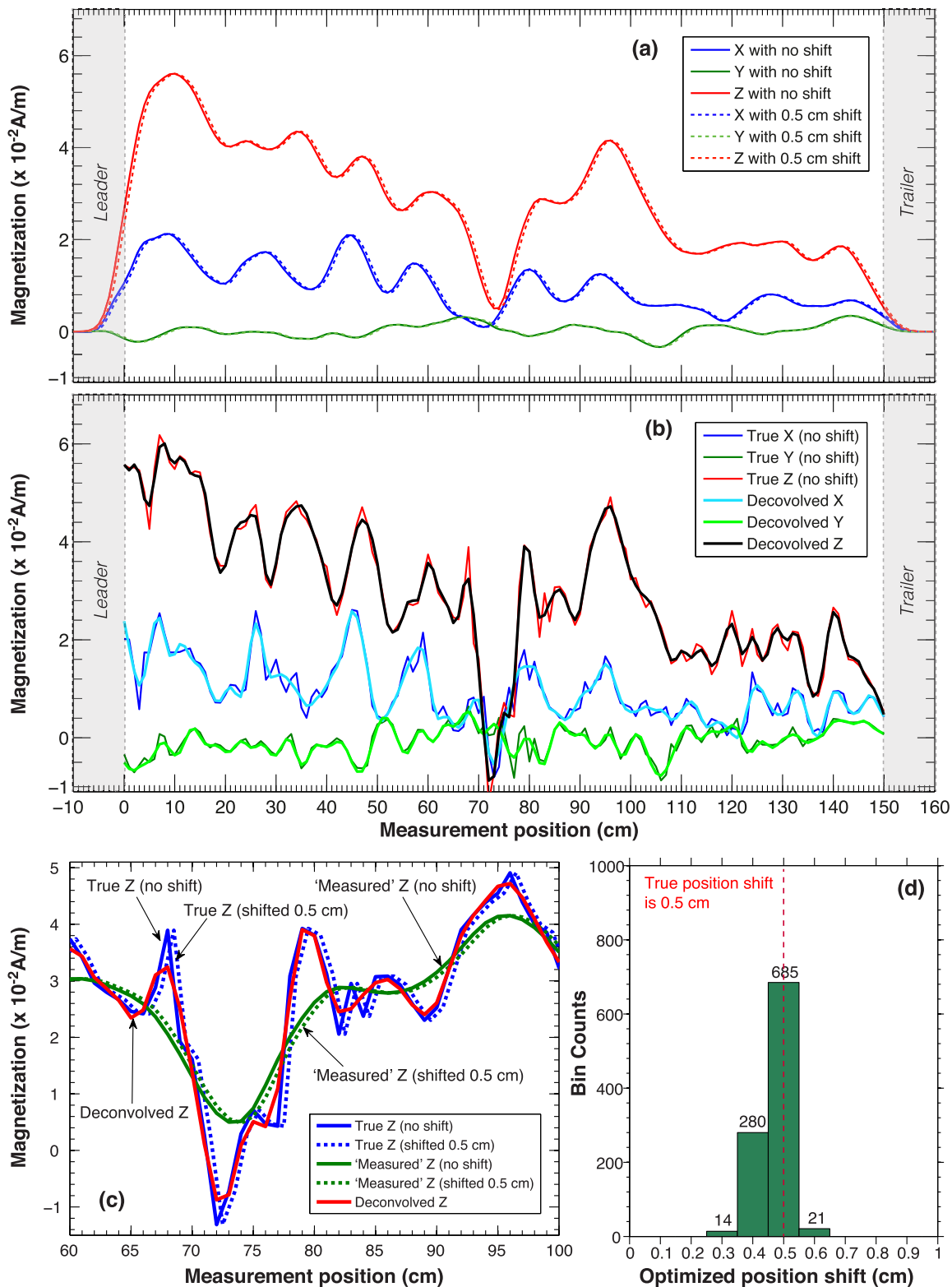


Figure 6. Test of position shift optimized deconvolution. (a) Synthetic “measured” magnetization with 0.5 cm (dashed lines) and without (solid lines) position shift in x (blue), y (red) and z axis (green). (b) An example of optimized deconvolution of the 1000 shifted synthetic measurements with realistic noise, compared with “true” signal without shift in x (light and dark blue curves), y (light and dark green curves) and z axis (black and red curves). (c) Blow-up of magnetization in z axis for the 60–100 cm interval before and after convolution and deconvolution. (d) Histogram of optimized position shift obtained from deconvolution of 1000 synthetic shifted measurements. Red vertical dashed lines indicate the true position shift of 0.5 cm.

mostly consistent with the “true” magnetization providing reasonable estimates of residuals and errors except slight discrepancies on measurement points with higher gradients of measured magnetic moment.

5.2. Optimization in Terms of Position Shift

To test the validity of optimization in terms of the new parameter “position shift,” deconvolution was performed for a second set of 1000 synthetic measurements that incorporates realistic measurement noise as well as a “position shift” of 0.5 cm (Figure 6). Optimization was conducted in terms of $\ln(u)$ and position shift at the same time to search for the combination of $\ln(u)$ and position shift that provides deconvolution result with a minimum ABIC. Figure 6b compares the “true” magnetization (with no shift) with one example of an optimized deconvolution result from the 1000 runs. The optimized deconvolution can clearly overcome the “position shift” introduced during the measurement even with the existence of realistic noise. A detailed comparison of the z axis magnetization between 60 and 100 cm with and without shift, before and after deconvolution is shown in Figure 6c. The optimized deconvolution result (solid red curve) tracks very well with the original true signal without shift (solid blue curve). The histogram in Figure 6d summarizes the optimized position shift values corresponding to the 1000 optimized deconvolution results, and clearly shows a peak around the “true” position shift of 0.5 cm. Optimization for the new parameter “position shift” improves the reliability of the deconvolution results by accounting for errors in placing a u-channel relative to the actual measurement “Start Line,” and accommodating possible void space in the beginning of a u-channel. The importance of having accurate positions of the u-channel in deconvolution was pointed out by Jackson *et al.* [2010], and our simulations suggest that such uncertainty can be accounted for using the new optimized deconvolution algorithm.

5.3. Optimization in Terms of Length Correction

In addition to “position shift,” we test the validity of deconvolution optimized for another new parameter “length correction” at the sample end, using a third set of 1000 synthetic measurements with realistic noise (Figure 7). In order to avoid instability of optimization at the end of the u-channel due to unusually low magnetization (therefore low signal-to-noise ratio), the same synthetic measurement data (before adding noise) used in Sections 5.1 and 5.2 were flipped along the z axis. The length correction of the last slice of synthetic magnetization was changed from zero (default length correction) to -0.3 cm (applied length correction) for the simulation, corresponding to a corrected u-channel length of 149.7 cm (“missing” 0.3 cm at the sample end). Optimization was conducted in terms of $\ln(u)$ and length correction at the same time to search for the combination of $\ln(u)$ and length correction that provides the deconvolution result with a minimum ABIC. Figure 7b compares the “true” magnetization (with no length correction) with one example of an optimized deconvolution result from the 1000 runs. The optimized deconvolution can apparently overcome the “missing” 0.3 cm of sediments with the existence of realistic noise, and restore the “true” magnetization at the sample end. A detailed comparison of the z axis magnetization between 130 and 160 cm with the default and applied length corrections, before and after deconvolution is shown in Figure 7c. The optimized deconvolution result (solid red curve) tracks very well with the original true signal without any “missing” material (solid blue curve). The histogram in Figure 7d summarizes the optimized length correction values corresponding to the 1000 optimized deconvolution results, and clearly shows a peak around the “true” length correction of -0.3 cm. Optimization for the new parameter “length correction” improves the reliability of the deconvolution results by reducing the uncertainty in practice due to the loss of sediment materials at the end of u-channel. A preliminary set of length correction optimization simulation using synthetic measurement records with a range of signal-to-noise (S/N) ratios suggest that absolute difference between the “true” and estimated length corrections is less than $\sim 0.5 \pm 0.8$ (1σ) mm for records with S/N ratios of $> \sim 10,000$, which are usually the case for most u-channel measurements. The optimization becomes less stable (with absolute difference of $\sim 1.7 \pm 1.4$ (1σ) mm) when S/N ratio of the measurement is reduced to ~ 100 . Although further study is needed for more robust evaluation of the stability of the algorithm, the preliminary simulation results suggest promising performance of the proposed length correction optimization for most u-channel measurement records with S/N ratios of $> \sim 10,000$.

6. Application to Real Data

To demonstrate the reliability of optimized deconvolution for real u-channel measurement data, we performed optimized deconvolution for 20 repeated measurements of u-channel EW0408-95JC-6 after 30 mT

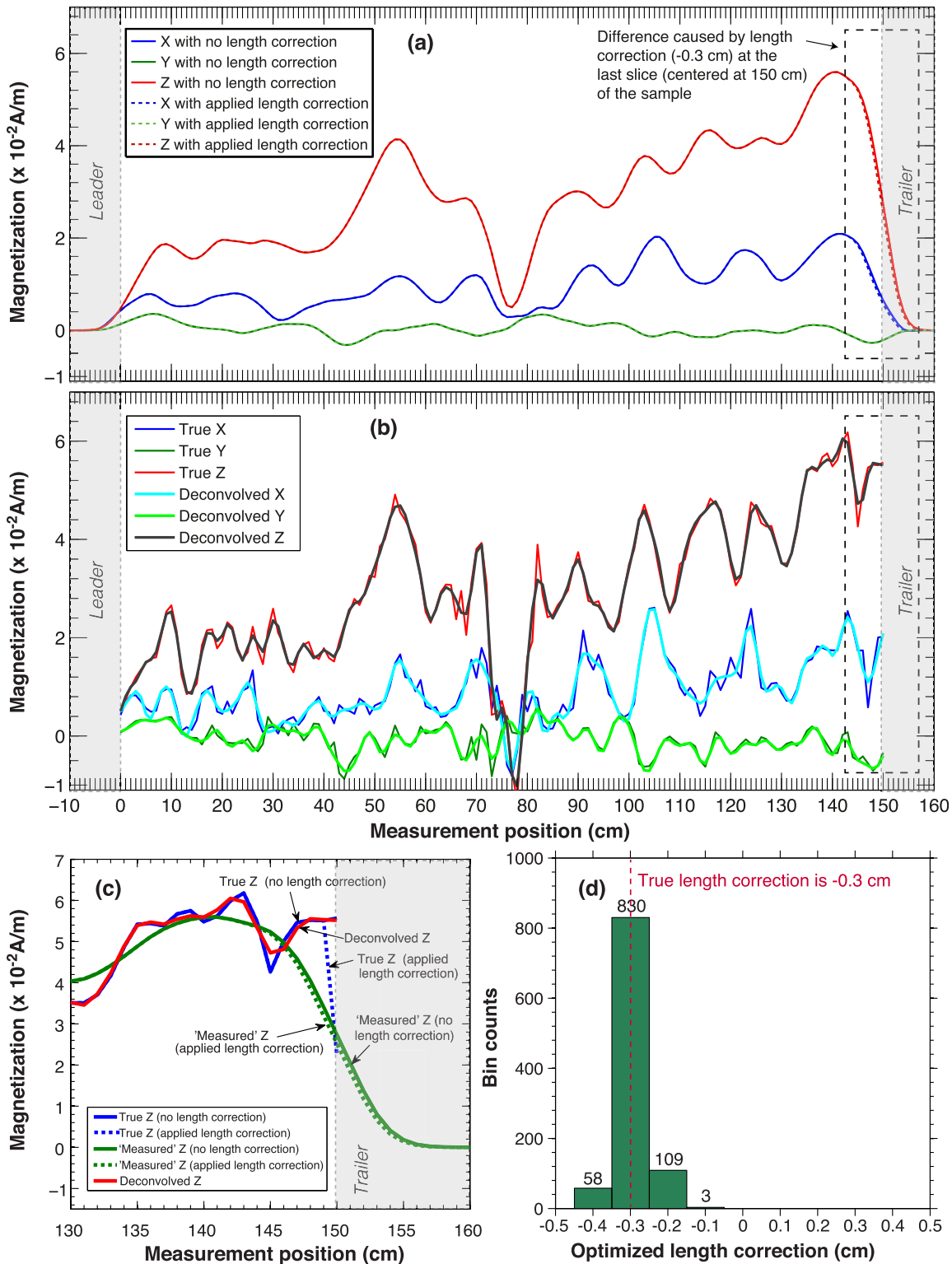


Figure 7. Test of deconvolution optimized for length correction. (a) Synthetic “measured” data in x (blue curves), y (red curves) and z axis (green curves), with applied (–0.3 cm; dashed lines) and default (0 cm; solid lines) length corrections at the right sample end. (b) An example of optimized deconvolution of the 1000 synthetic measurements with applied length correction and added noise, compared with synthetic true signal in x (light and dark blue curves), y (light and dark green curves) and z axis (black and red curves). (c) Blowup of magnetization in z axis for the 130–160 cm interval before and after convolution and deconvolution. (d) Histogram of optimized length correction obtained from deconvolution of the 1000 synthetic measurements. Red vertical dashed lines indicate the true applied length correction of –0.3 cm.

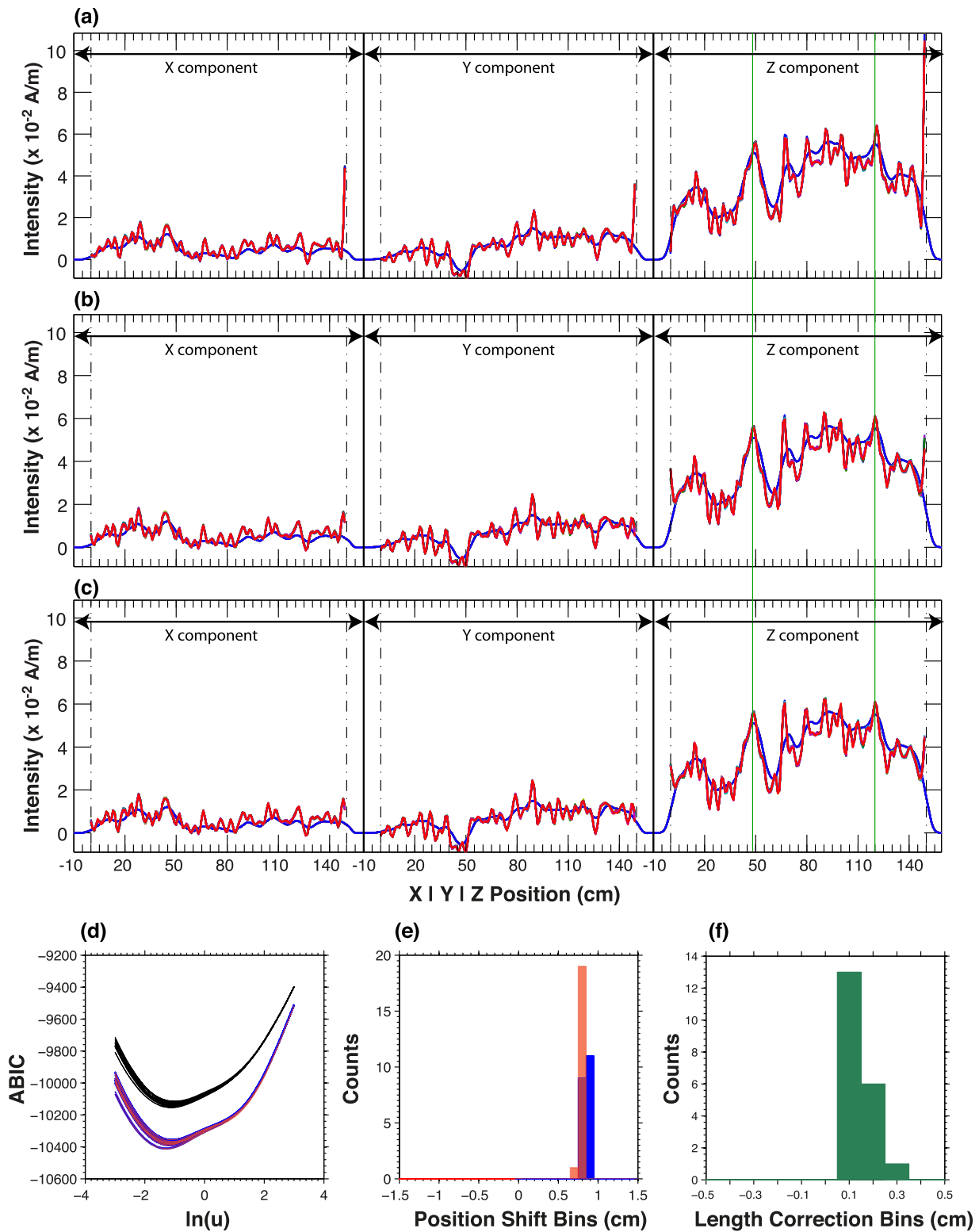


Figure 8. Deconvolution of 20 repeated measurements of u-channel sample “EW0408-95JC-6” (after 30 mT AF demagnetization) optimized for (a) $\ln(u)$ only, (b) $\ln(u)$ and position shift, (c) $\ln(u)$, position shift, and length correction. Vertical dot dashed lines indicate the end of leader or beginning of trailer measurements. (d) $\ln(u)$ versus ABIC plot for deconvolution of each repeated measurement. For deconvolution in Figure 8b and 8c, only results associated with optimized position shift and/or length correction are shown. (e) Histogram of optimized position shift values for deconvolution of the 20 measurements. Blue and red bars are from optimized deconvolution in Figure 8b and 8c, respectively. (f) Histogram of optimized length correction values from optimized deconvolution in Figure 8c.

AF demagnetization (Figure 8). For each measurement step, deconvolution was optimized only for $\ln(u)$ first (Figure 8a), then optimized for $\ln(u)$ and position shift (Figure 8b), and finally optimized for $\ln(u)$, position shift, and length correction (Figure 8c). Ranges used for the optimized deconvolution are -3 to 3 (with 0.2 step) for $\ln(u)$, -1.5 cm to 1.5 cm (with 0.1 cm step) for position shift, and -0.5 cm to 0.5 cm (with 0.1 cm step) for length correction, respectively. Figures 8a–8c compare the 20 repeated measurements before (blue curves) and after optimized deconvolution (red curves). It is clear that deconvolved data for the 20 repeated measurements are highly consistent with each other using any of the three optimized deconvolution schemes (i.e., $\ln(u)$ only, $\ln(u)$ and position shift, and all three parameters), suggesting that optimized deconvolution can reliably restore high-resolution information for measurement data with realistic errors.

Results of deconvolution using the three different optimization schemes are generally comparable to each other, but with apparent differences especially near the ends of the sample. For instance, deconvolution optimized only for $\ln(u)$ of the 20 repeated measurements (red curves in Figure 8a) shows a significant increase at the right end of the sample in all three axes. This abnormal increase in the magnetization was significantly reduced in deconvolution results optimized for both $\ln(u)$ and position shift (Figure 8b), and for all three parameters (Figure 8c). A small relative shift (<1 cm) can also be observed in the deconvolved data between Figure 8a and Figure 8b, as well as between Figure 8a and Figure 8c (see vertical green lines in Figure 8). The improvements in the solution can also be monitored on the $\ln(u)$ against ABIC value plots for each of the 20 deconvolution runs (Figure 8d). Minimum ABIC values for deconvolution optimized for $\ln(u)$ and position shift (blue), and for all three parameters (red) show values much smaller than that optimized for $\ln(u)$ only (black).

As the u -channel sample was not moved during the 20 repeated measurements, “true” position shift and length corrections of the 20 runs should be very similar to each other. Figure 8e shows the consistency of the optimized position shift values for deconvolution of the 20 repeated measurements. All 20 runs of deconvolution optimized for $\ln(u)$ and position shift yield optimized position shifts of either 0.8 cm (9 runs) or 0.9 cm (11 runs) (blue), and 19 of the 20 runs of deconvolution optimized for all three parameters yielded an optimized position shift of 0.8 cm (red). Figure 8f shows the optimized length correction values for deconvolution of 20 repeated measurements optimized for all three parameters. The results show a major peak at 0.1 cm (13 out of 20 runs), and smaller peaks at 0.2 cm (6 out of 20 runs) and 0.3 cm (only 1 run). The small value of length correction might be the reason for the similarities in deconvolved magnetization and minimum ABIC for deconvolution optimized for $\ln(u)$ and position shift, and for all three parameters. The consistency in optimized position shift and length correction values for the results of 20 repeated measurements indicate that optimized deconvolution can be achieved and is stable considering realistic measurement uncertainties.

7. Conclusions

High quality sensor response estimate was acquired for superconducting rock magnetometer (SRM) at Oregon State University (OSU) based on repeated (150 times) measurements of a precisely fabricated magnetic point source placed at 25 different positions on a cross section in three orthogonal orientations, over an ~ 40 cm interval along the track at every 1 mm intervals. A new deconvolution algorithm was devised incorporating new parameters “position shift” and “length correction” along with Akaike’s Bayesian Information Criterion (ABIC) minimization of *Oda and Shibuya* [1996]. Analyses on repeated measurements (200 times) of a u -channel sample after 10 step-wise AF demagnetization treatments indicate that the standard deviation of measurement error is related to the gradient of measured magnetic moment.

The algorithm is tested using synthetic measurement data constructed by convolving the sensor response with a “true” magnetization resampled from a sedimentary paleomagnetic record containing an excursion. A total of 1000 simulated noise was superimposed on the synthetic measurement records by randomly taking standard deviation values according to the distribution of standard deviation for a certain gradient of measured magnetic moment acquired from repeated measurements. Deconvolution of the 1000 simulated signals closely resembles the true signal, and successfully restores the excursion that is not observable before deconvolution. Optimization for “position shift” using synthetic data with realistic noise and a “true” shift of 0.5 cm successfully reduced the error of deconvolution at the ends of the sample, and the deconvolved data tracks the true magnetization very well. Optimized “position shift” values are mostly consistent

with the true value of 0.5 cm. Optimization for “length correction” using synthetic data with realistic noise and a void interval (−0.3 cm) at the sample end clearly yield deconvolved magnetizations that track the true magnetization very well. A majority of the 1000 optimized “length correction” values match the true value of −0.3 cm. Deconvolution of 20 repeated real measurements indicates that optimized deconvolution can be achieved and results are stable considering realistic measurement uncertainties. In order to obtain more reliable magnetization by deconvolution, a practically designed standard point source, and convenient software for sensor response optimization, as well as precise positioning are needed.

Acknowledgments

The authors would like to express their sincere thanks to Hideki Yoshikawa for the fabrication of a standard point source, and to Nobuyoshi Natsuhara for providing plastic magnet powder and calibration of the spinner magnetometer. The authors are grateful to William Goree for providing information on SRM. Jun Kawai kindly provided information on SQUID systems in general. The authors are also indebted to the encouragements and many supports from Joseph Stoner, James E.T. Channell, and Toshitsugu Yamazaki. This research was partially supported by Grant-in-Aid for Scientific Research (A) 25247082, JSPS, Japan provided to Hirokuni Oda. Chuang Xuan was supported by startup grants provided by the Oregon State University and the University of Southampton. All data presented in this paper are available for request by emailing the authors.

References

- Acton, G. D., M. Okada, B. M. Clement, S. P. Lund, and T. Williams (2002), Paleomagnetic overprints in ocean sediment cores and their relationship to shear deformation caused by piston coring, *J. Geophys. Res.*, *107*(B4), 2067, doi:10.1029/2001JB000518.
- Channell, J., and Y. Guyodo (2004), The Matuyama Chronozone at ODP Site 982 (Rockall Bank): Evidence for decimeter-scale magnetization lock-in depths, in *Timescales of the Internal Geomagnetic Field*, AGU Geophys. Monogr. 145, edited by J. E. T. Channell et al., pp. 205–219, AGU, Washington, D. C.
- Channell, J. E. T., D. A. Hodell, and B. Lehman (1997), Relative geomagnetic paleointensity and $\delta^{18}\text{O}$ at ODP Site 983 (Gardar Drift, North Atlantic) since 350 ka, *Earth Planet. Sci. Lett.*, *153*, 103–118, doi:10.1016/S0012-821X(97)00164-7.
- Channell, J. E. T., C. Xuan, and D. A. Hodell (2009), Stacking paleointensity and oxygen isotope data for the last 1.5 Myr (PISO-1500), *Earth Planet. Sci. Lett.*, *283*, 14–23, doi:10.1016/j.epsl.2009.03.012.
- Constable, C., and R. Parker (1991), Deconvolution of longcore palaeomagnetic measurements—Spline therapy for the linear problem, *Geophys. J. Int.*, *104*, 453–468, doi:10.1111/j.1365-246X.1991.tb05693.x.
- Dodson, R. E., M. D. Fuller, and W. Pilant (1974), On the measurement of the remanent magnetism of long cores, *Geophys. Res. Lett.*, *1*, 185–188, doi:10.1029/GL001i004p00185.
- Goree, W. S., and M. D. Fuller (1976), Magnetometers using RF-driven SQUIDs and their applications in rock magnetism and paleomagnetism, *Rev. Geophys.*, *14*, 591–608.
- Goree, W. S. (2007), Rock magnetometer, superconducting, in *Encyclopedia of Geomagnetism and Paleomagnetism*, edited by D. Gubbins and E. Herrerobervera, pp. 883–886, Springer, Dordrecht, Netherlands.
- Guyodo, Y., and J. P. Valet (1999), Global changes in intensity of the Earth’s magnetic field during the past 800 kyr, *Nature*, *36*, 234–238.
- Guyodo, Y., J. E. T. Channell, and R. G. Thomas (2002), Deconvolution of u-channel paleomagnetic data near geomagnetic reversals and short events, *Geophys. Res. Lett.*, *29*(17), 1845, doi:10.1029/2002GL014927.
- Helmholtz, H. V. (1849), *Vortrag in der Sitzung*, vol. 16, III, Physikalische Ges., Berlin; Loeb, L. B. (1947), *Fundamentals of Electricity and Magnetism*, 3rd ed., John Wiley, New York.
- Jackson, M., J. A. Bowles, I. Lascu, and P. Solheid (2010), Deconvolution of u channel magnetometer data: Experimental study of accuracy, resolution, and stability of different inversion methods, *Geochem. Geophys. Geosyst.*, *11*, Q07Y10, doi:10.1029/2009GC002991.
- Oda, H., and H. Shibuya (1994), Deconvolution of whole-core magnetic remanence data by ABIC minimization, *J. Geomagn. Geoelectr.*, *46*, 613–628.
- Oda, H., and H. Shibuya (1996), Deconvolution of long-core paleomagnetic data of Ocean Drilling Program by Akaike’s Bayesian Information Criterion minimization, *J. Geophys. Res.*, *101*, 2815–2834, doi:10.1029/95JB02811.
- Oda, H., and H. Shibuya (1998), An improvement in ABIC-minimizing deconvolution for continuously measured magnetic remanence data, *Earth Planets Space*, *59*, 15–22.
- Oda, H., H. Shibuya, and V. Hsu (2000), Palaeomagnetic records of the Brunhes/Matuyama polarity transition from ODP Leg 124 (Celebes and Sulu seas), *Geophys. J. Int.*, *142*, 319–338, doi:10.1046/j.1365-246x.2000.00130.x.
- Ohno, M., F. Murakami, F. Komatsu, Y. Guyodo, G. Acton, T. Kanamatsu, H. F. Evans, and F. Nanayama (2008), Paleomagnetic directions of the Gauss-Matuyama polarity transition recorded in drift sediments (IODP Site U1314) in the North Atlantic, *Earth Planets Space*, *60*, e13–e16.
- Parker, R. L., and J. S. Gee (2002), Calibration of the pass-through magnetometer-II. Application, *Geophys. J. Int.*, *150*, 140–152, doi:10.1046/j.1365-246X.2002.01692.x.
- Roberts, A. P. (2006), High-resolution magnetic analysis of sediment cores: Strengths, limitations and strategies for maximizing the value of long-core magnetic data, *Phys. Earth Planet. Inter.*, *156*, 162–178, doi:10.1016/j.pepi.2005.03.021.
- Shibuya, H., and T. Michikawa (2000), Calculation of superconducting rock magnetometer response, *Kumamoto J. Sci. Earth Sci.*, *16*, 1–16.
- Suganuma, Y., J. Okuno, D. Heslop, A. P. Roberts, T. Yamazaki, and Y. Yokoyama (2011), Post-depositional remanent magnetization lock-in for marine sediments deduced from ^{10}Be and paleomagnetic records through the Matuyama-Brunhes boundary, *Earth Planet. Sci. Lett.*, *311*, 39–52, doi:10.1016/j.epsl.2011.08.038.
- Tauxe, L., J. L. Labrecque, D. Dodson, and M. Fuller (1983), “U”channels - a new technique for paleomagnetic analysis of hydraulic piston cores, *EOS Trans. AGU*, *64*, 219.
- Valet, J.-P., L. Meynadier, and Y. Guyodo (2005), Geomagnetic dipole strength and reversal rate over the past two million years, *Nature*, *435*, 802–805, doi:10.1038/nature03674.
- Weeks, R., C. Laj, L. Endignoux, M. Fuller, A. Roberts, R. Manganne, E. Blanchard, and W. Goree (1993), Improvements in long-core measurement techniques: Applications in palaeomagnetism and palaeoceanography, *Geophys. J. Int.*, *114*, 651–662.
- Xuan, C., and J. E. T. Channell (2009), UPmag: MATLAB software for viewing and processing u channel or other pass-through paleomagnetic data, *Geochem. Geophys. Geosyst.*, *10*, Q10Y07, doi:10.1029/2009GC002584.
- Zięba, A. (1993), Image and sample geometry effects in SQUID magnetometers, *Rev. Sci. Instrum.*, *64*, 3357–3375, doi:10.1063/1.1144306.